

Supplementary Information

Micro- and nano-patterned elastin-like polypeptide hydrogels for stem cell culture

A. Paul,^{a,†,*} M. Stührenberg,^{a,†} S. Chen,^b D. Rhee,^c W.-K. Lee,^c T. W. Odom,^{c,d} S. C. Heilshorn^b and A. Enejder^a

^a Department of Biology and Biological Engineering, Chalmers University of Technology, Gothenburg 41296, Sweden.

^b Department of Materials Science and Engineering, Stanford University, Stanford, CA 94305, United States.

^c Department of Materials Science and Engineering, Northwestern University, Evanston, IL 60208, United States.

^d Department of Chemistry, Northwestern University, Evanston, IL 60208, United States.

† denotes equal contribution. *Correspondence to: alexandra.paul@chalmers.se

Content

Supplementary Tables

Table S1. Amino acid sequence of the ELP biomaterial.

Table S2. Overview of wavelengths and amplitudes of produced PDMS molds and ELP samples.

Supplementary Figures

Figure S1. Characterization of the lower critical solution temperature (LCST) of ELP.

Figure S2. Stiffness (E_c) of flat ELP substrates characterized by AFM.

Figure S3. CARS and Raman spectrum of a crosslinked 5 wt% ELP hydrogel.

Figure S4 Representative CARS and AFM images of 1D PDMS molds, dry and hydrated ELP hydrogels.

Figure S5. Representative CARS and AFM images of 2D PDMS molds, dry and hydrated ELP hydrogels.

Figure S6. Actin and nuclear staining of ADSC after 24 h on the ELP scaffolds and evaluation of alignment.

Supplementary Methods

Method S1. Detailed description of the FFT algorithm used for automated extraction of wavelengths from AFM and CARS images (**Figure S7**).

References

- 1 K. S. Straley and S. C. Heilshorn, *Soft Matter*, 2009, **5**, 114.

Supplementary Tables

Table S1. Amino acid sequence of ELP.¹



Symbol	Module name	Amino acid sequence
T7	T7 Tag	MASMTGGQQMG
His	Histidine Tag	HHHHH
EK	Enterokinase cleavage site	DDDDK
Bio	Cell-adhesive	TVYAVTGRGDSPASSAA
Elastin	Elastin-like	[(VPGIG) ₂ VPKG(VPGIG) ₂] ₃ VP

Table S2. Measured surface topography of aligned (1D) and unaligned (2D) patterns on PDMS molds and dehydrated ELP substrates measured with AFM and CARS.

	$\lambda_{\text{PDMS,AFM}}$ [μm]	$h_{\text{PDMS,AFM}}$ [μm]	$\lambda_{\text{ELP,AFM}}$ [μm]	$h_{\text{ELP,AFM}}$ [μm]	$\lambda_{\text{ELP,CARS}}$ [μm]
1D	3.97	0.69±0.3	3.73	0.54±0.16	4.3
	2.29	0.39±0.19	2.40	0.29±0.16	1.8
	2.12	0.42±0.22	1.64	0.28±0.09	1.4
	1.52	0.40±0.18	1.35	0.30±0.14	1.4
	1.19	0.30±0.18	1.42	0.28±0.05	1.4
	0.73	0.26±0.17	0.84	0.17±0.07	1.0
	0.60	0.17±0.11	0.60	0.13±0.04	-
	0.55	0.046±0.017	0.37	0.05±0.03	-
	0.24	0.016±0.011	-	-	-
2D	4.54	1.06±0.18	4.32	0.94±0.47	4.7
	2.57	0.82±0.45	2.15	0.53±0.30	2.2
	1.35	0.29±0.10	1.35	0.22±0.08	1.4
	0.84	0.12±0.06	0.81	0.11±0.04	1.2
	0.60	0.14±0.06	0.48	0.11±0.09	-
	0.40	0.16±0.07	0.40	0.07±0.04	-
	0.43	0.048±0.02	-	-	-

Supplementary Figures

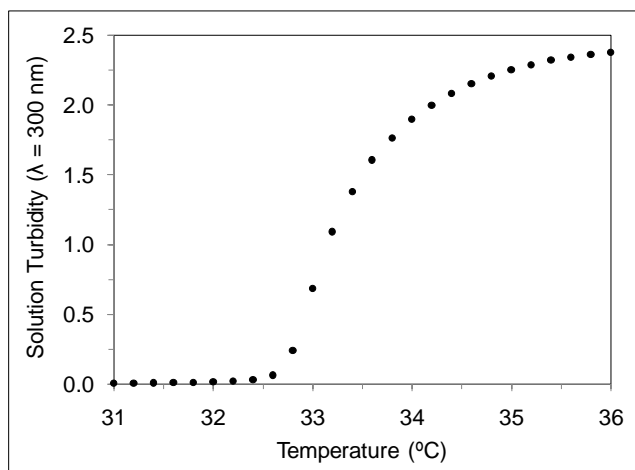


Figure S1. Characterization of the lower critical solution temperature (LCST) of ELP.¹ Lyophilized protein was resuspended at a concentration of 10 mg/mL in phosphate buffered saline (PBS, pH = 7.2, 4°C). Turbidity readings at 300 nm were monitored as a function of temperature using a Molecular Devices SpectraMax Plus384 Spectrophotometer. The temperature was increased at a rate of 0.1°C/min with an equilibration time of 30 s at each step. The LCST is taken as the inflection point in the turbidity curve, which occurs at 33.3°C.

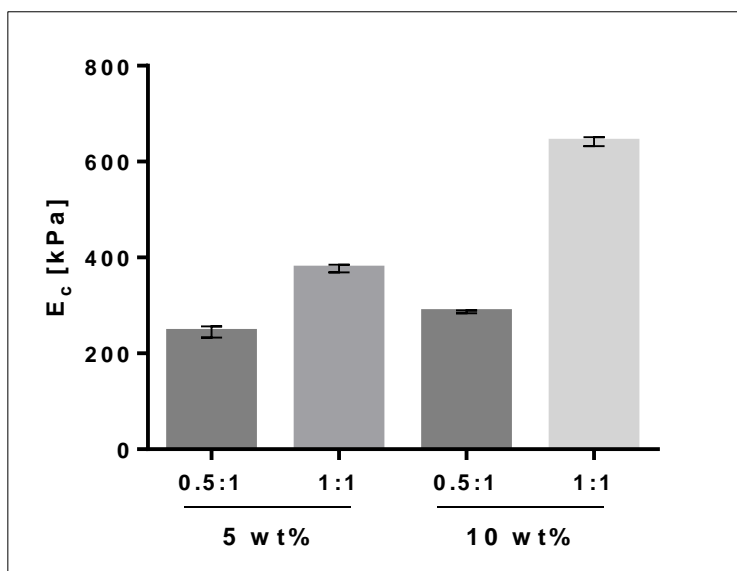


Figure S2. Stiffness (E_c) of flat ELP substrates characterized by AFM. For atomic force microscopy (AFM) measurements, ELP crosslinked coatings were formed within a confined, 10-mm diameter spread area using silicone sheet molds (Electron Microscopy Sciences). Samples were prepared as described in the main text to yield 5 wt% ELP with a 1:1 stoichiometric ratio of crosslinker functional group to primary amines within the ELP. For comparison, additional samples with a 0.5:1 stoichiometric ratio at 5 wt% ELP and 1:1 and 0.5:1 ratios at 10 wt% ELP are included. Samples were rehydrated and measured while submerged in PBS. Short silicon contact mode probes (Applied NanoStructures) were used to collect measurements using 1 μm force distance, 1 Hz scanning rate, 0.5 V trigger point, and an internal gain of 10. Data was fit using the Hertz indentation model for a cone-tip geometry, assuming a Poisson ratio of 0.4. Data are presented as averages with standard error of mean, $n > 10$. All values are significantly different as evaluated with ANOVA with post-hoc Tukey test.

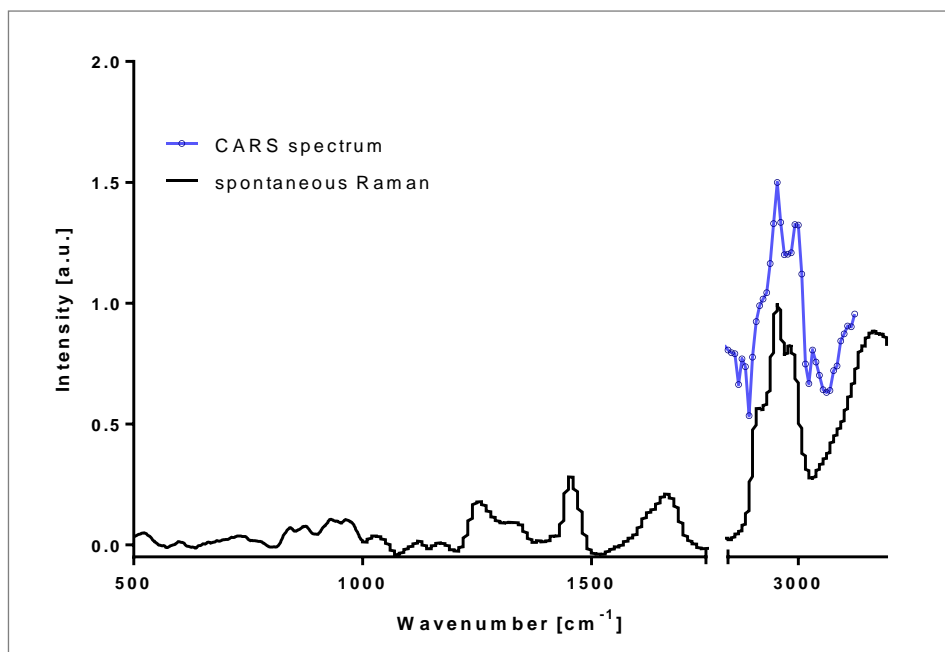
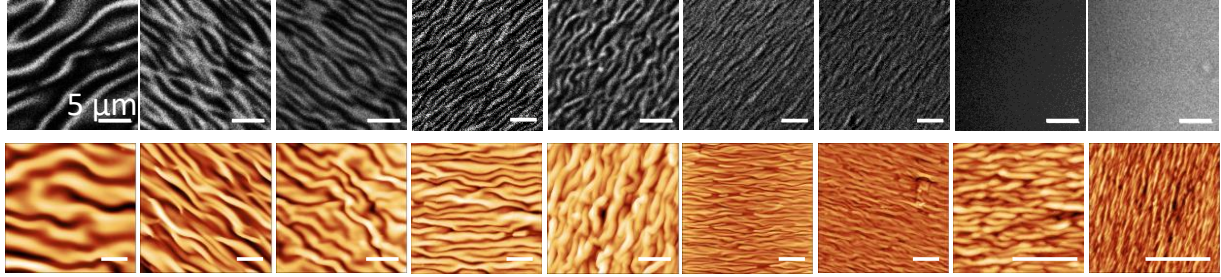


Figure S3. CARS (blue) and Raman (black) spectra of a crosslinked 5 wt% ELP hydrogel. Both spectra are normalized to 2930 cm⁻¹ and the CARS spectrum is presented with an offset.

A – PDMS

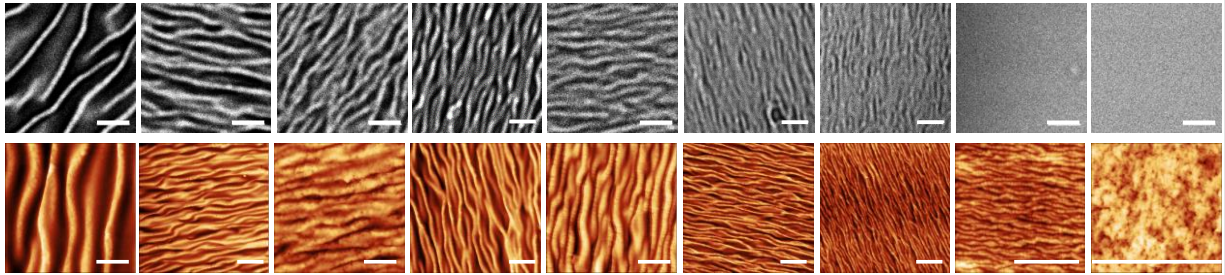
Pattern size

3.97 μm 2.29 μm 2.12 μm 1.52 μm 1.19 μm 0.73 μm 0.60 μm 0.55 μm 0.24 μm



B – ELP

3.73 μm 2.40 μm 1.64 μm 1.35 μm 1.42 μm 0.84 μm 0.60 μm 0.37 μm -



C – hydrated ELP

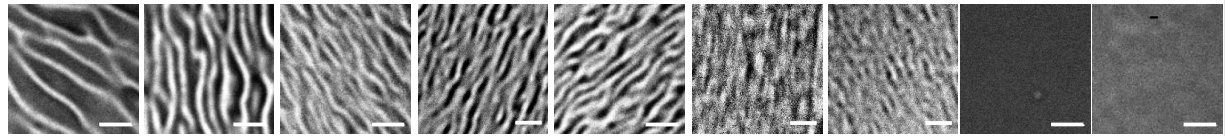


Figure S4. Overview of CARS (grey) and AFM (gold) images of the different aligned (1D) samples: PDMS molds (A), dehydrated ELP substrates (B), hydrated ELP substrates (C). (Scale bar: 5 μm)

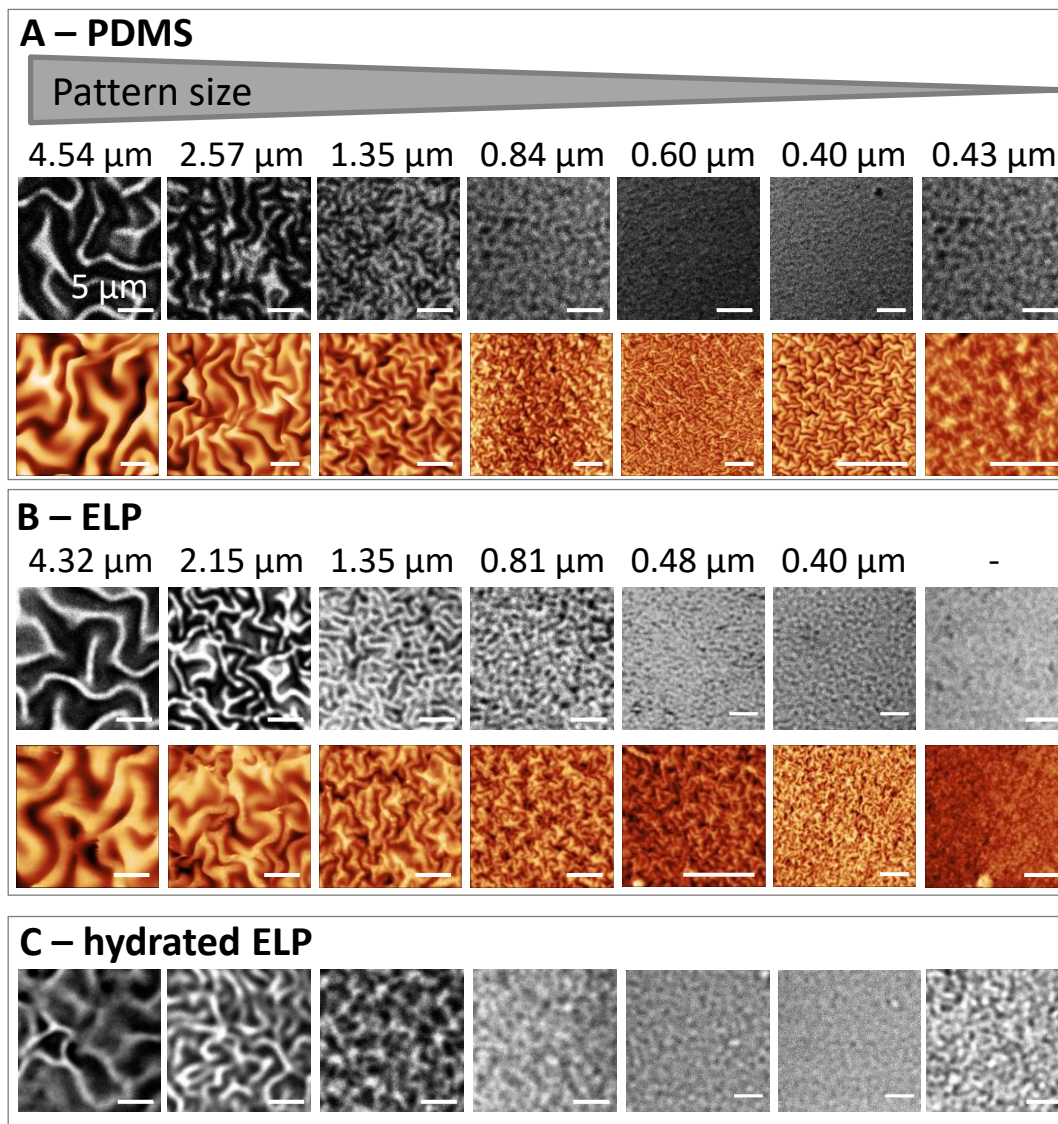


Figure S5. Overview of CARS (grey) and AFM (gold) images of the different unaligned (2D) samples: PDMS molds (A), dehydrated ELP substrates (B), hydrated ELP substrates (C). (Scale bar: 5 μm)

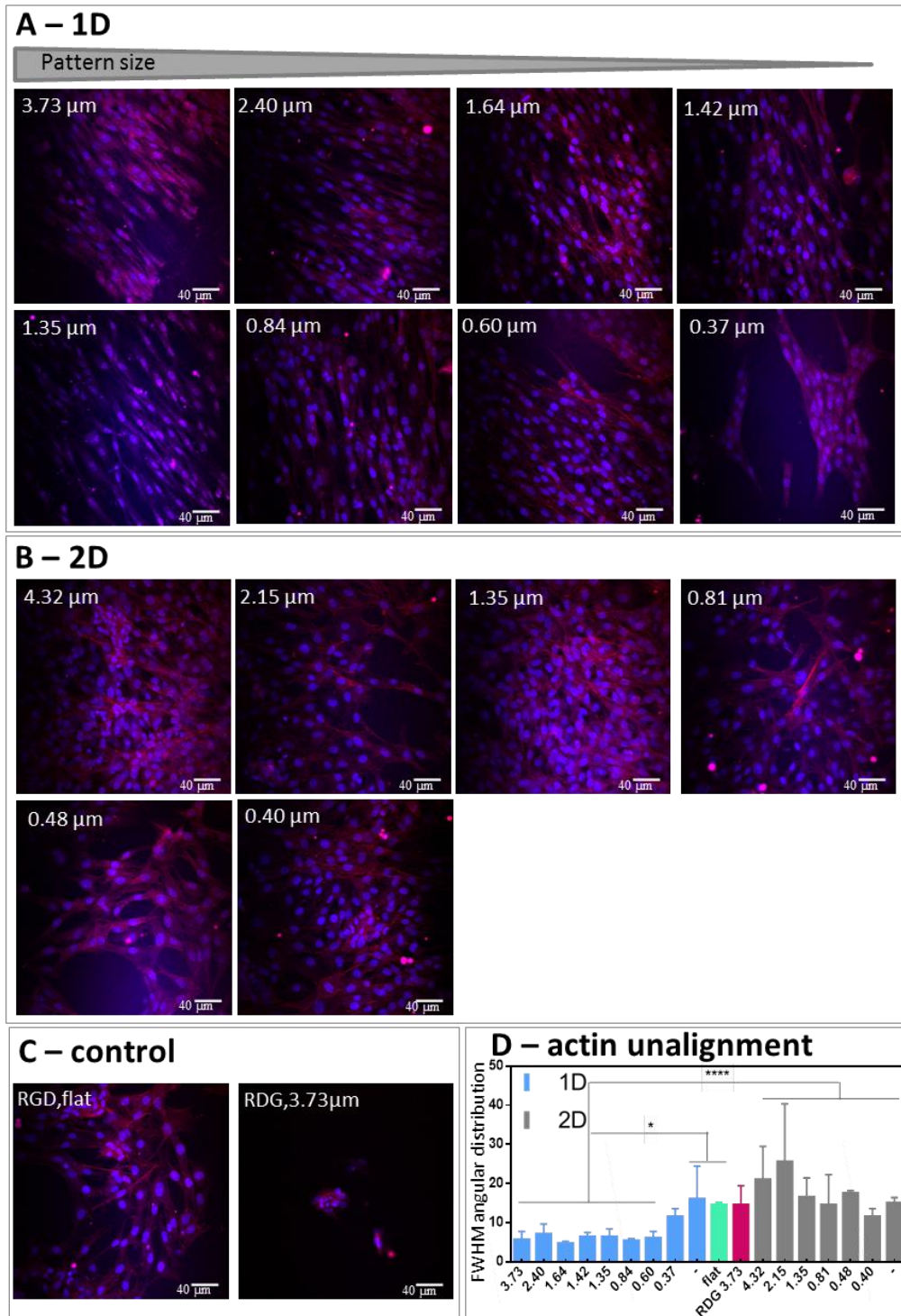


Figure S6. A,B: Cells show different adhesion patterns on the 1D (A) and 2D (B) nanowrinkled ELP hydrogels 24h after seeding (actin filaments in red via TPEF microscopy of Phalloidin-Alexa488, nuclei in blue via TPEF microscopy of Hoechst33342). C: Cells also adhere to flat substrates with RGD-ELP (left) but hardly to hydrogels containing RDG-ELP (right). D: Quantification of FWHM of the angular distribution of the actin filaments with statistically significant difference between the 1D and 2D group ($P < 0.0001$) and 1D and flat samples ($P = 0.02$). Values displayed as mean \pm SD. (Scale bar: 40 μ m)

Supplementary Methods

Method S1. Detailed description of the FFT algorithm used for automated extraction of wavelengths from AFM and CARS images.

To determine the average wavelength of the wavy samples (both aligned 1D patterns as well as unaligned 2D patterns), we used the image analysis software Fiji. First, the images were converted to 8-bit (Fig. 7 a,b) and then transformed into a binary mask by applying 'local thresholding' with the method 'mean'(Fig. S7 c,d). In order to match the local threshold radius with the unknown wrinkle wavelength, a series of different radii was used per image. From these binary masks, the fast Fourier transform (FFT) algorithm, included in Fiji, was applied to transform the spatial information to the frequency domain (Fig. S7 e,f). The FFT data then was integrated radially outwards via the 'Radial Profile' plugin and fitted with a Gaussian function (Fig. S7 g,h):

$$f(r) = a \cdot e^{-\frac{(r-b)^2}{c^2}} + d \quad (1)$$

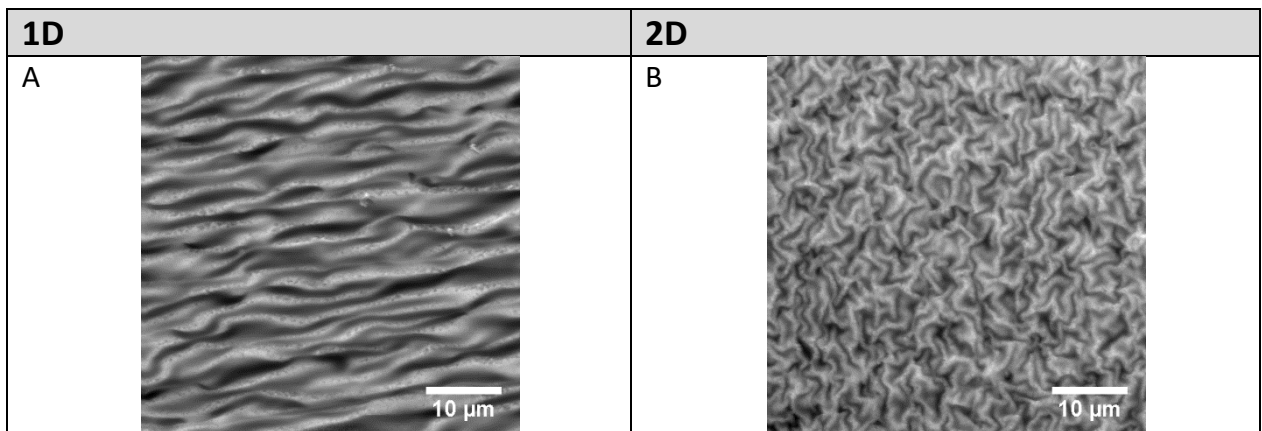
where b is the maximum of the fit function and corresponds to the average wavelength of each mask. Plotting these wavelengths shows a saturation trend for smaller threshold radii which can be fit by a sigmoidal function (Fig. S5, i,j):

$$y(x) = \frac{g}{1 + e^{-\frac{x-h}{j}}} + k \quad (2)$$

We extrapolate the sigmoidal function to the smallest threshold radius:

$$\lim_{x \rightarrow 0} y(x) = y_0 = \lambda_{wrinkle} \quad (3)$$

And determined y_0 as the optimal wavelength.



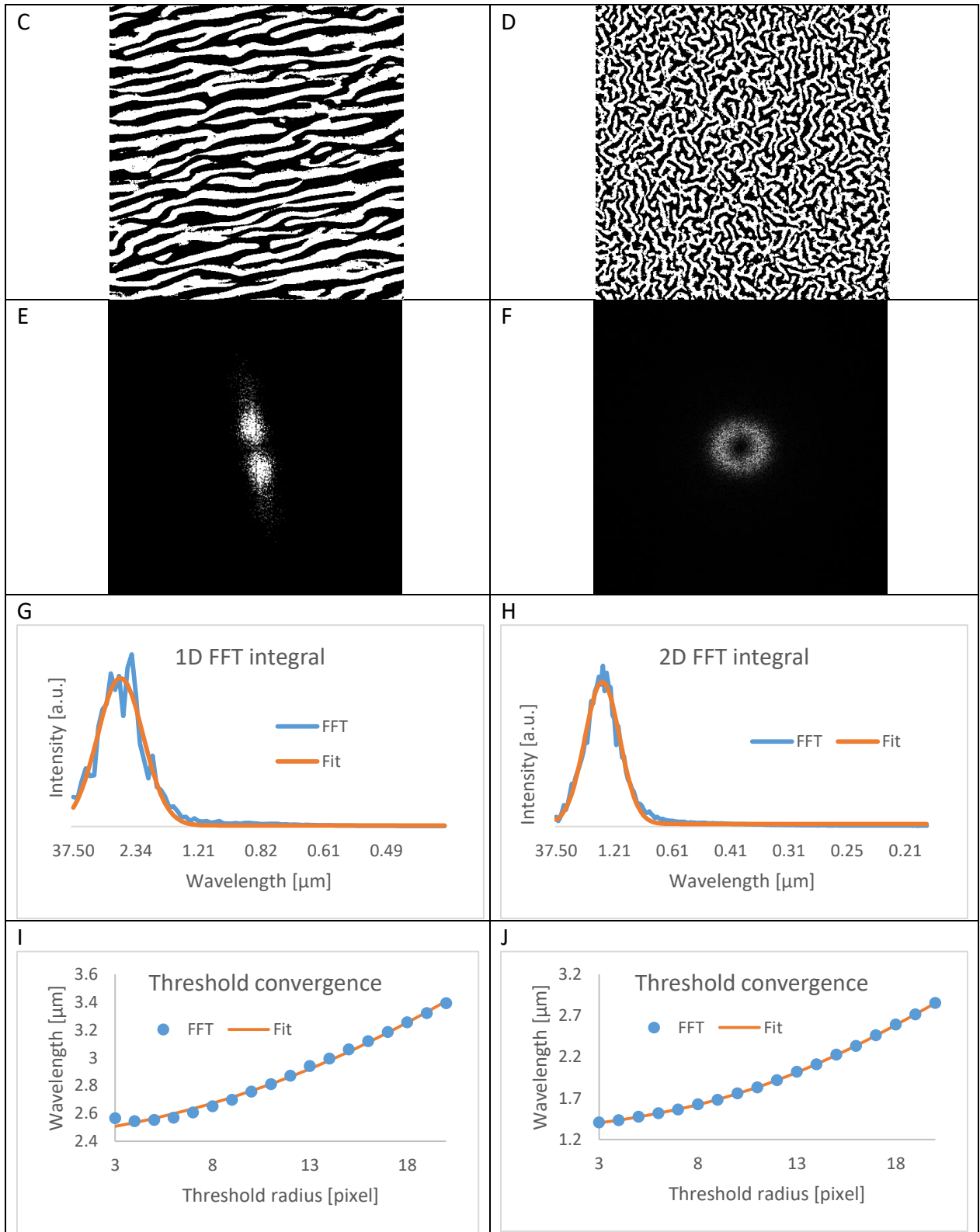


Figure S7. A,B: Original AFM scans. C,D: Binary mask from images in A,B. E,F: Images from the Fourier domain. G,H: Integrated FFT with Gaussian fit. I,J: Threshold convergence for optimal wavelength determination. Final wavelengths are λ_{1D} = 2.40 μm and λ_{2D} = 1.35 μm